Applied Catalysis B: Environmental 202 (2017) 104–111

Contents lists available at ScienceDirect

Applied Catalysis B: Environmental

journal homepage: www.elsevier.com/locate/apcatb

Facile synthesis of a novel full-spectrum-responsive $Co_{2.67}S_4$ nanoparticles for UV-, vis- and NIR-driven photocatalysis

Zhenzhen Wu[a,b], Xingzhong Yuan[a,b,*], Hou Wang[a,b,*], Zhibin Wu[a,b], Longbo Jiang[a,b], Hui Wang[a,b], Lei Zhang[a,b], Zhihua Xiao[c], Xiaohong Chen[d], Guangming Zeng[a,b]

[a] College of Environmental Science and Engineering, Hunan University, Changsha 410082, PR China
[b] Key Laboratory of Environment Biology and Pollution Control, Hunan University, Ministry of Education, Changsha 410082, PR China
[c] College of Bioscience and Biotechnology, Hunan Agricultural University, Changsha, 410128, PR China
[d] Hunan University of Commerce, Changsha 410205, PR China

ARTICLE INFO

Article history:
Received 20 June 2016
Received in revised form 8 August 2016
Accepted 30 August 2016
Available online 3 September 2016

Keywords:
Photocatalytic
Full-spectrum
$Co_{2.67}S_4$ nanoparticles
Near-infrared
Methylene blue

ABSTRACT

Sparked by growing pollution issues, research aiming at a better harvesting of solar energy in photocatalysts for environmental remediation has been thriving. In this study, a novel mixed valence state of $Co_{2.67}S_4$ nanoparticles with full-spectrum-responsive photocatalytic activity had been fabricated via a facile solvothermal route. The as-synthesized samples were systematically characterized by scanning electron microscopy (SEM), transmission electron microscopy (TEM), X-ray diffraction (XRD), X-ray photoelectron spectroscopy (XPS) and UV–vis-NIR diffuse reflection spectroscopy (UV–vis-NIR DRS). The photocatalytic performance of as-obtained samples had been investigated by the degradation of methylene blue (MB) in aqueous solution. The $Co_{2.67}S_4$ nanoparticles with the particle size of 5–20 nm could degrade MB with the efficiency of 64%, 84% and 68% under the UV light, visible light and near-infrared light exposure, respectively. Furthermore, a possible photocatalytic mechanism toward the near-infrared region had been proposed to be that the Co^{2+}/Co^{3+} redox couple played vital parts in the photocatalytic activity of $Co_{2.67}S_4$. This study provides a novel full solar spectrum-responsive photocatalyst for solar-light utility and environmental remediation.

1. Introduction

As a free, abundant and non-polluting resource, solar energy has been deemed as one of the most promising renewable energy sources all over the world [1–4]. For the better use of solar energy, numerous investigations of photocatalysts have been implemented [5–7]. However, it is still a challenging task to exploit a photocatalytic materials with efficient broad spectrum harvesting and conversion for solar light, especially the near-infrared (NIR) wavelength [8–10]. So far, the response of photocatalysts have been mostly confined in the spectrum from UV to visible wavelength, whereas the near-infrared light which reaches nearly 44% in the solar spectrum has been rarely harvest [11–15].

The pioneering investigations of such near-infrared light photocatalysts have been basically focused on the up-conversion luminescence of rare earth materials for the past 30 years. Upon the near-infrared excitation at 980 nm, the rare earth materials could generate upconverted emission peaks changing from near-infrared to UV or visible region of the spectrum [16–21]. Served as an intermedium, the up-conversion materials can convert NIR excitation light into visible or UV emission light to excite corresponding photocatalysts. After that, the forceful oxidative holes and reductive electrons could be generated for the photocatalytic reaction [12,16]. Nevertheless, the quantum efficiency of up-conversion photocatalyst was limited, owing to its extremely narrow absorption band of light at 980 nm [22,23]. Therefore, many other photocatalysts which possessed Vis-NIR or NIR photocatalytic activity come into being, such as WS_2, Bi_2WO_6 and $Cu_2(OH)PO_4$ [24,25]. However, to date, $Co_{2.67}S_4$ photocatalyst, a kind of transition-metal sulfides with full-spectrum-responsive photocatalytic activity, has not been investigated.

Recently, the transition-metal sulfides were regarded as a type of promising candidates, owing to the distinctive and irreplaceable cracking electronic, magnetic, and photovoltaic properties in energy, catalysis, and electricity [26–29]. Cobalt sulfides (Co_mS_n), a significant kind of complicated transition-metal sulfides, possess

* Corresponding authors at: College of Environmental Science and Engineering, Hunan University, Changsha 410082, PR China.
E-mail addresses: yxz@hnu.edu.cn (X. Yuan), huankewanghou024@163.com (H. Wang).

http://dx.doi.org/10.1016/j.apcatb.2016.08.064
0926-3373/

diverse chemical formulas and various crystalline phases, such as CoS_2, CoS, Co_9S_8, Co_3S_4, Co_3S_2, and $Co_{1-x}S$ [27,30–32]. Moreover, Co_mS_n have exhibited excellent potentiality in energy storage and conversion devices, such as electrochemical capacitors, catalysts for fuel cells, dye-sensitized solar cells and cathode materials for lithium-rechargeable batteries [33–35]. Furthermore, the quantum chemical calculations revealed that the surface structure of Co_mS_n (e.g., CoS) could create electron transfer pathways for oxygen reduction kinetics, which facilitated for the improvement of catalytic activity [36]. Up to now, most investigations of Co_mS_n have been focused on the electrochemistry, and rarely utilized in photocatalysis and waste-water treatment.

Recently, our group had reported the facile synthesis of Sb_2S_3/ultrathin g-C_3N_4 sheets heterostructures embedded with g-C_3N_4 quantum dots with enhanced NIR-light photocatalytic performance [37]. Besides, metal sulfides-based composites including $Sb_2S_3/Sb_4O_5Cl_2$, In_2S_3@MIL-125(Ti), SnS_2-$MgFe_2O_4$/rGO and metal sulfides quantum dots on MIL-125(Ti) had been synthesized by hydrothermal method, solvothermal method and photodeposition strategy, respectively. These photocatalysts had shown excellent visible light photocatalytic activity [38–42]. In this study, a novel full-spectrum-response photocatalyst $Co_{2.67}S_4$ was fabricated by a facile solvothermal method, which exhibited great optical absorption in a broad range of 240–2200 nm, covering the wave band of UV, visible and NIR region. The obtained photocatalysts were characterized by SEM, TEM, XRD, XPS and UV–vis-NIR DRS [43]. The $Co_{2.67}S_4$ nanoparticles with mixed valence had realized great photocatalytic property for methylene blue (MB) degradation under UV, visible and NIR irradiation. The degraded MB wastewater samples were characterized by three dimensional fluorescence excitation-emission matrix (3D EEM) and gas chromatography-mass spectrometry (GC–MS). Moreover, a possible mechanism toward the near-infrared light has been proposed.

2. Experimental section

2.1. Materials

Cobalt chloride ($CoCl_2{\cdot}6H_2O$), Sodium sulfide ($Na_2S{\cdot}9H_2O$), Ethylene glycol ($C_2H_6O_2$) and Methylene blue (MB, $C_{16}H_{18}N_3SCl$) were purchased from Sinopharm Chemical Reagent Co., Ltd. (Shanghai, China). All chemicals were of analytical grade and used as received without any further purification.

2.2. Synthesis of $Co_{2.67}S_4$ nanoparticles

$Co_{2.67}S_4$ nanoparticles were synthesized by means of a facile solvothermal procedure. In general, 1 mmol of $CoCl_2{\cdot}6H_2O$ and 2.2 mmol of $Na_2S{\cdot}9H_2O$ were dissolved in 40 mL ethylene glycol at room temperature. Then, the mixtures were stirred for 30 min to form a homogeneous solution. Afterwards, all of the mixtures were transferred into a 50 mL Teflon-lined autoclave for 24 h at 150 °C, 180 °C and 200 °C. When the autoclave cool to room temperature, the as-synthesized black products were collected by centrifugation, washed with distilled water and absolute ethanol, subsequently, to remove any ionic residual. Finally, the products were dried under vacuum at 60 °C overnight.

2.3. Characterization

The powder X-ray diffraction (XRD) patterns of $Co_{2.67}S_4$ nanoparticles were carried out with Bruker AXS D8 advance diffractometer operating with Cu-Ka radiation (λ = 1.5406 Å) to investigate the crystal structure of the samples under 40 kV, 250 mA. The surface elemental composition and valence state of the sample was implemented by X-ray photoelectron spectroscopy (XPS), which were recorded on a Thermo ESCALAB 250Xi instrument, and the binding energies of adventitious carbon (284.8 eV) were applied for charge correction. Transmission electron microscopy (TEM, JEOL JEM-1230) and scanning electron microscope (SEM, JEOL JSM-6700) images were applied to investigate the morphology and structure of the obtained samples. The materials was uniformly dispersed into absolute ethanol by ultrasound method, and the solution was evenly dropped on the copper grids. After drying, the copper grids was observed by Transmission electron microscopy (TEM), the chemical composition was examined via energy-dispersive X-ray spectroscopy (EDS) attached to the TEM. UV–vis-NIR diffuse reflectance spectra (UV–vis-NIR DRS) of the samples were recorded on a UV–vis-NIR spectrophotometer (U4100, Hitachi) with an integrating sphere attachment within the range of 240–2200 nm and $BaSO_4$ was used as the reflectance standard.

2.4. Photocatalytic activity test

The photocatalytic activities of the $Co_{2.67}S_4$ nanoparticles were estimated by the photodegradation of MB under UV, visible and near-infrared light irradiations supplied by a 300 W Xenon lamp (Beijing China Education Au-light, Co., Ltd.). The light source (14 V, 16 A, 15 cm) far away from the photocatalytic reator. Typically, the photocatalytic degradation was actualized in a 250 mL beaker, containing 100 mL MB solution (10 mg L^{-1}) and 50 mg photocatalyst. To dispel the effect of adsorption on the experimental results, the solutions were magnetically stirred for one hour in a dark condition to achieve the adsorption-desorption equilibrium under room air conditions. Moreover, a 300 W Xenon lamp was applied as the UV light, visible light and near-infrared light source, under assistance of filters to ensure the light < 400 nm as UV source, light of 400–760 nm as visible source as well as the light < 760 nm were cut off by filter as near infrared source. Every periodic interval of 20 min, 4 mL aliquots were drawn out and centrifuged to remove the particles. The residual MB concentrations were detected at 664 nm by a UV–vis spectrophotometer (UV-2250, SHIMADZU Corporation, Japan). In the experiment of oxidative species detection, the holes, $^{\bullet}OH$ and $^{\bullet}O_2^-$ generated during the photocatalytic process were resolved by sodium oxalate, isopropanol and N_2-saturated condition respectively. The degraded MB wastewater samples were characterized by EEM spectroscopy (F-4600, Hitachi). Scanning emission spectra was acquired from 200 to 800 nm by varying the excitation wavelength from 200 to 800 nm at 10 nm increments. The chemical constituents of the dichloromethane extract of degraded MB wastewater samples were determined by GC–MS analysis. GC–MS was run on a GCMS-QP2010 Plus spectrometer (30 m × 0.25 mm × 0.25 μm; SHIMADZU, Japan) with helium (2.0 mL/min) as carrier gas.

3. Results and discussions

3.1. Characterizations on $Co_{2.67}S_4$ nanoparticles

Firstly, the crystal phase compositions and purity of as-obtained samples were characterized by X-ray diffraction (XRD), as shown in Fig. 1. It can be clearly seen that all of the diffraction peaks could be well corresponded with the cubic phase of $Co_{2.67}S_4$, which matched well with the standard XRD patterns (PDF#97-010-9368), and no impurity peaks were identified. Moreover, the lattice parameters could be calculated to be a = 9.44 Å, and the XRD spectrum also showed four peaks located at 2θ = 31.4°, 38.1°, 50.2° and 55.0°, corresponding to the (311), (400), (511) and (440) planes of $Co_{2.67}S_4$. After photodegradation, no obvious changes of the XRD patterns

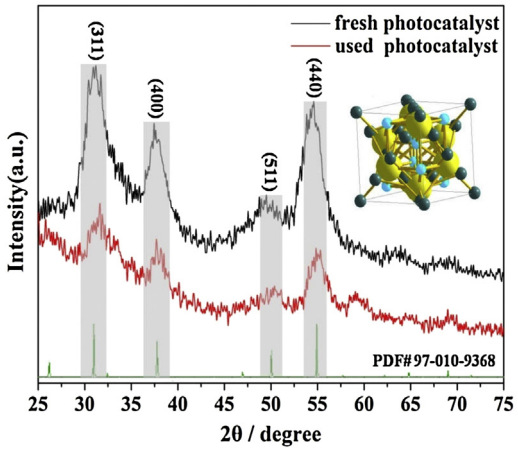

Fig. 1. The XRD pattern of $Co_{2.67}S_4$ sample. (Reference: $Co_{2.67}S_4$, JCPDS No.109368). The unit cell crystal structure of $Co_{2.67}S_4$ is shown in the middle right inset.

could be observed, indicating the well stability of $Co_{2.67}S_4$ nanoparticles during photocatalytic process.

The scanning electron microscopy (SEM) images of $Co_{2.67}S_4$ nanoparticles prepared at 150 °C, 180 °C and 200 °C were shown in Fig. 2(a–c). It could be found that the solvothermal temperature of raw materials acted as a significant role in influencing the sizes and morphologies of the $Co_{2.67}S_4$ nanoparticles. With the increase of reaction temperature, the surface of sample became more smoothly. To characterize the fascinating microstructures more specifically, the $Co_{2.67}S_4$ nanoparticles prepared at 180 °C were further confirmed by TEM, as shown in Fig. 2(d,e). This clearly exhibited that the $Co_{2.67}S_4$ nanoparticles were granular in morphology with a primary particle size of 5–20 nm. The atom-scale dispersion of starting materials might contribute to the regularity and homogeneity of final products [44]. The HRTEM image in Fig. 2e displays the distinct and uniform lattice fringes with fixed crystallographic orientation, indicating the high crystallinity of $Co_{2.67}S_4$. The well-defined lattice interplanar spacings of around 0.167 and 0.236 nm were attributed to the distances of (440) and (400) crystal planes of $Co_{2.67}S_4$, respectively. Besides, energy-dispersive X-ray spectroscopy (EDS) was implemented to confirm the chemical composition. The EDS image (Fig. 2f) indicated that the nanoparticles were composed of Co and S elements. The molar ratio of S and Co had been calculated to be nearly 1.5, which was extremely close to the refinement results and stoichiometric $Co_{2.67}S_4$, coinciding with the XRD results. Besides, the other main peak of EDS (Fig. 2f) was composed of Cu elements in the copper grids.

X-ray photoelectron spectroscopy (XPS) was used to characterize the valent state of the elements in $Co_{2.67}S_4$. The XPS spectrum exhibited S 2p and Co 2p signals with a S/Co ratio of nearly 1.5, which was approximate to the theoretical value of $Co_{2.67}S_4$. Fig. 3a shows the Co 2p high-resolution XPS spectra, which had been attentively fitted and analyzed considering the spin-orbit. The Co 2p XPS spectra demonstrated that the core level spectrum of Co 2p region had been deconvoluted into two spin-orbit doublets. The main peaks, having a Co $2p_{1/2}$ at 792.9 eV and a Co $2p_{3/2}$ at 777.8 eV, could be attributed to the Co atoms being in a +3 oxidation state [45,46]. The second doublet, with a binding energy at 796.4 eV and 780.2 eV, could be ascribed to the emission of Co $2p_{1/2}$ and Co $2p_{3/2}$ core levels from the Co atoms in an oxidation state of +2 [47,48]. Meanwhile, two broad peaks observed at 801.7 eV and 784.7 eV might be attributed to the satellite peaks of Co 2p, which were accorded well with the reported values [49]. It was indicated the existence of

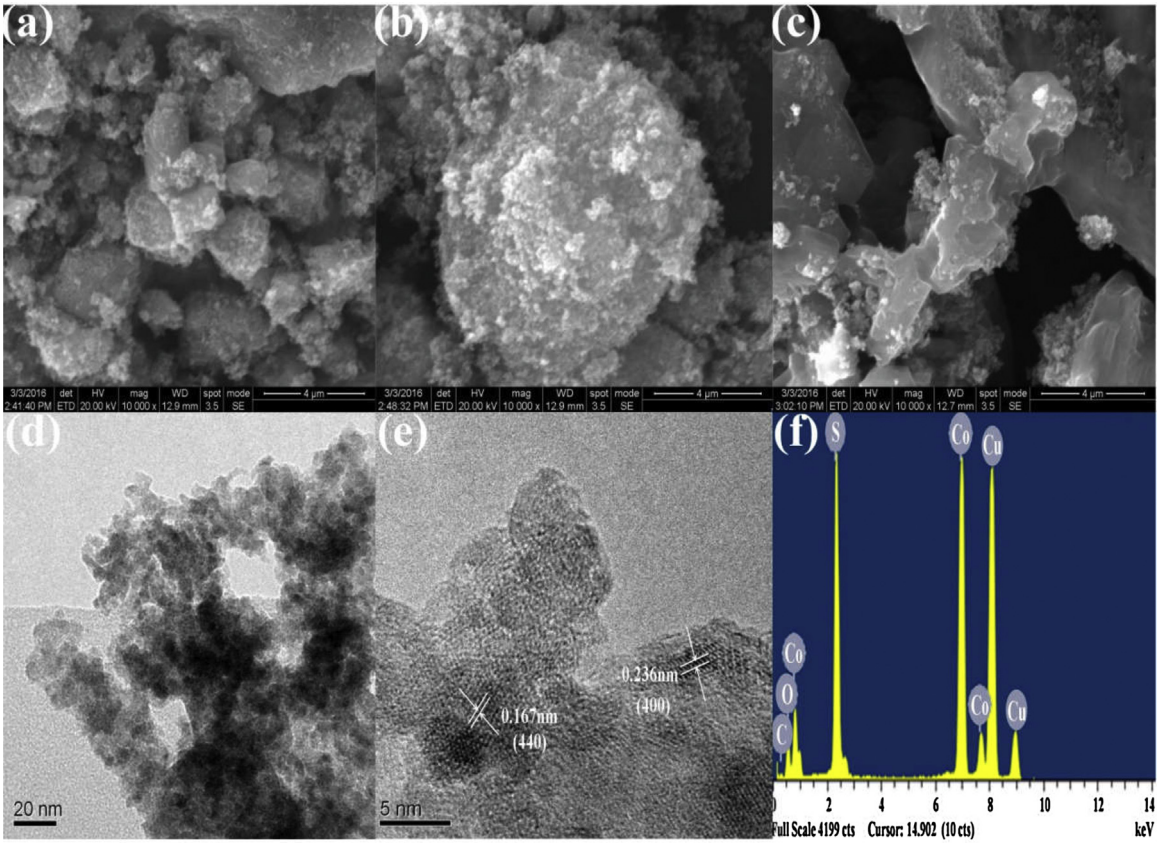

Fig. 2. (a-c) ESEM image of prepared $Co_{2.67}S_4$ at 150 °C, 180 °C, 200 °C for 24 h. (d) TEM image, (e) HRTEM image and (f) EDX analysis of $Co_{2.67}S_4$ nanoparticles.

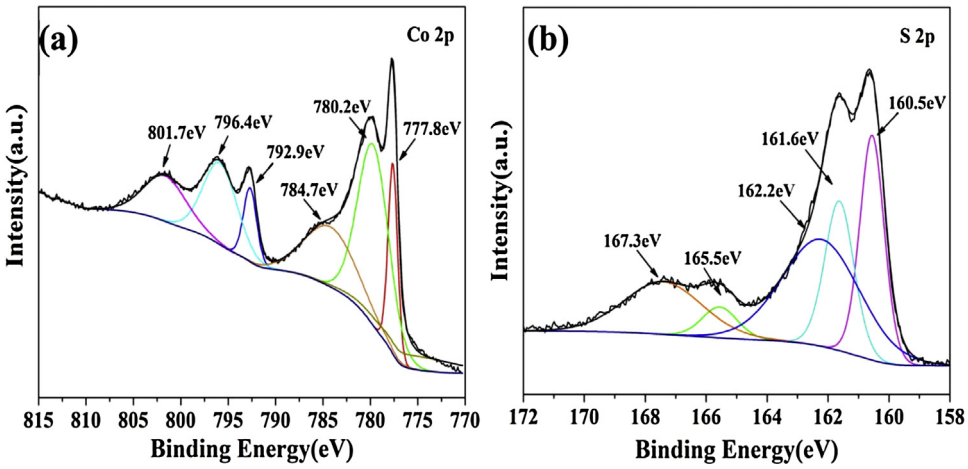

Fig. 3. XPS spectra of (a) Co 2p and (b) S 2p for $Co_{2.67}S_4$ nanoparticles.

two chemically obvious species: Co (III) and Co (II). From the S 2p signal in Fig. 3b, the peaks situated at binding energies of 160.5 eV, 161.6 eV and 162.2 eV could be assigned to S 2p, while the peak at binding energy of ~167.3 eV was attributed to the shake-up satellite (sat.) structure [50]. On the other hand, the emission peak at 165.5 eV can be assigned to the Co-S-thiolate bonds accounting for only 3.3%, which were not broken completely to form Co-S bonds of $Co_{2.67}S_4$ during the process of synthesis [26]. The detailed ball-stick models of the $Co_{2.67}S_4$ structure were shown in Fig. 4(a,b). The cell of $Co_{2.67}S_4$ was presented as a cube, which could be also in agreement with the XRD results. According to the results of XRD, SEM, TEM and XPS, it can be inferred that $Co_{2.67}S_4$ nanoparticles had been successfully synthesized.

The UV–vis-NIR diffuse reflectance spectra (UV–vis-NIR DRS) of the samples were measured and shown in Fig. 5. The DRS absorption spectra (Fig. 5a) reveals that the $Co_{2.67}S_4$ nanoparticles had exhibited obvious optical absorption in the solar region of 240–2200 nm, especially for the NIR light of 760–2200 nm. The absorption edge of the $Co_{2.67}S_4$ apparently tailed out to the NIR range without extinction. The results could define the $Co_{2.67}S_4$ as a "NIR-sensitive" structure [51]. The band gap energy could be computed from the formula $(\alpha h\nu)^{1/2} \propto h\nu - E_g$, where α, h, ν, and E_g were absorption coefficient, Planck's constant, light frequency, and band gap energy, respectively. Moreover, the band gap energy of $Co_{2.67}S_4$ had been evaluated to be 0.92 eV (Fig. 5b). The DRS absorption spectra distinctly revealed that the optical absorption of $Co_{2.67}S_4$ had been shifted towards NIR light wavelengths, which was highly necessary for exploring the full-spectrum-response photocatalytic activity.

3.2. Photocatalytic performance of $Co_{2.67}S_4$

In order to prove the photocatalytic activity of the $Co_{2.67}S_4$, the degradation of methylene blue (MB) in aqueous solution under UV-, vis-, NIR light had been implemented. The degradation rate of MB was calculated by $(1 - C/C_0) \times 100\%$, where C (mg/L) was the concentration of MB at the irradiation time t (min) and C_0 (mg/L) was the concentration of MB after dark reaction one hour. Firstly, the degradation efficiency of MB for the prepared $Co_{2.67}S_4$ at 150 °C, 180 °C and 200 °C under near-infrared irradiation for 120 min were determined to be 38%, 68% and 60%, respectively (Fig. 5c). The phenomenon clearly indicated that the best reaction temperature for the synthesis of $Co_{2.67}S_4$ could be 180 °C. To further verify the full-spectrum-response photocatalytic performance of $Co_{2.67}S_4$, the temporal variations of absorption spectra of dye solutions under UV light and visible light were also shown in Fig. 5d. The photodegradation efficiency of MB over $Co_{2.67}S_4$ nanoparticles was more than 64% within 60 min under UV light irradiation. $Co_{2.67}S_4$ nanoparticles exhibited highest photocatalytic activities for photodegradation of MB under visible light irradiation for 60 min, the degradation efficiency was determined to be approximately 84%. For comparison, only a negligible amount of the MB had been degraded in the absence of photocatalyst. As a result, it further confirmed the full-spectrum-response photocatalytic properties of $Co_{2.67}S_4$ nanoparticles.

The 3D EEM fluorescence spectra of the treated solution before or after NIR light irraditaion with $Co_{2.67}S_4$ at different time had been measured. Previous to irradiation, two characteristic fluorescence

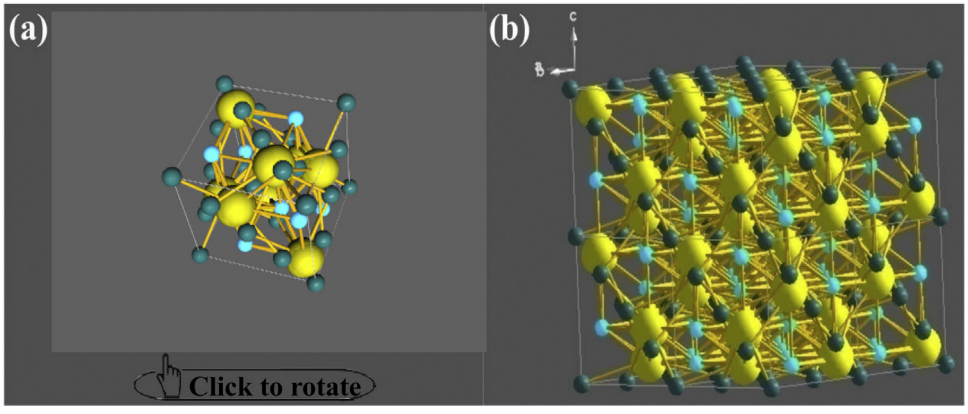

Fig. 4. (a) 3D-unit cell crystal structure of $Co_{2.67}S_4$ nanoparticles, (b) $2 \times 2 \times 2$ cells crystal structure of $Co_{2.67}S_4$ nanoparticles (green, blue, and yellow balls represent Co^{2+}, Co^{3+}, and S atoms, respectively). (For interpretation of the references to colour in this figure legend, the reader is referred to the web version of this article.)

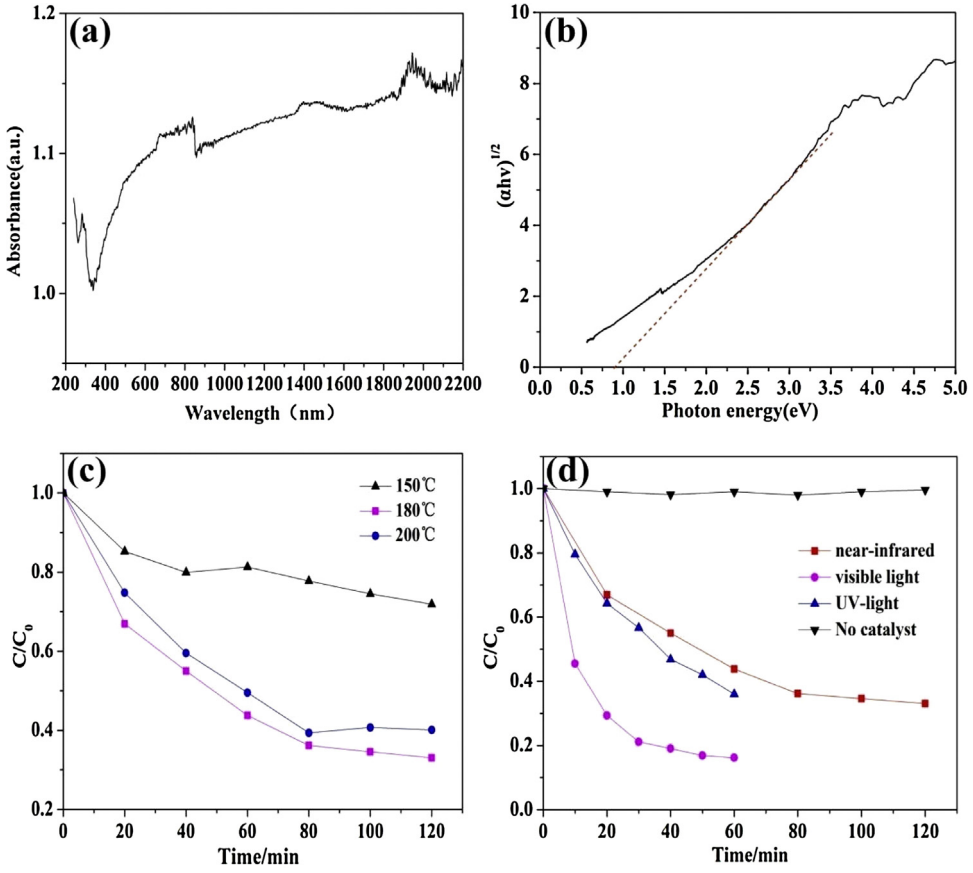

Fig. 5. (a) UV–vis-NIR diffuse reflectance spectra of $Co_{2.67}S_4$. (b) the corresponding plots of the $(ah\nu)^{1/2}$ versus photon energy ($h\nu$) for $Co_{2.67}S_4$. (c) Comparison of photocatalytic activities of prepared $Co_{2.67}S_4$ at 150 °C, 180 °C, 200 °C for 24 h on the degradation of MB under near-infrared irradiation. (d) photocatalytic degradation of MB in the presence of $Co_{2.67}S_4$ nanoparticles under UV light, visible light, and near-infrared light irradiation, and without catalyst for comparison tests.

peaks had been contained principally in MB (Fig. 6a). As shown in Fig. 6b, the fluorescence intensity of MB remains unchanged after the dark reaction for one hour. In the first degradation of 60 min (Fig. 6c), all the characteristic fluorescence peaks intensities of MB had decreased gradually, and two same characteristic peaks were distinctly displayed. When the NIR light irradiation time extended to 120 min, the peak intensity of MB continued to decrease, even nearly disappear (Fig. 6d). Based on the decreased fluorescence intensity, it could be revealed that not only the decolorization reaction occurred but also the MB was degraded during the irradiation of NIR light. To further identify the degradation products of the MB under NIR light irradiation, the degraded MB wastewater samples were detected by GC–MS. The main chemical constituents of the degraded MB are exhibited in Table 1. The major chemical components identified were heptadecanoic acid, methyl ester and methyl stearate; dodecane, 2-methyl-6-propyl. Consequently, it clearly revealed that the $Co_{2.67}S_4$ nanoparticles could be as a promising materials for dye waste-water cleaning.

3.3. Full-spectrum-responsive photocatalytic degradation mechanism of $Co_{2.67}S_4$

In the early stage, the photocatalytic degradation mechanism of dye by photocatalysts under the UV or visible light irradiation has been well established as follows. The light with higher energy than bandgap of photocatalysts was absorbed and then induced a

Table 1
Main chemical constituents of the dichloromethane extract of MB after NIR light irradiation 120 min as determined by GC–MS analysis.

Chemical constituents	Retention time (min)
3-*n*-Heptyl-7-methyl-9-(2,6,6-trimethylcyclohex-1-enyl)nona-2,4,6,8- tetraenal	12.82
3-Methyl-7-(4-methyl-piperazin-1-yl)-3H-thiazolo[4,5-*d*]pyrimidine-2- thione	12.91
Lanosta-7,9(11)-dien-18-oic acid, 22,25-epoxy-3,17,20-trihydroxy-, gamma. -lactone, (3.beta.)	13.79
Imidazole-2-carboxylic acid, 1-methyl	14.59
Triacontanoic acid, methyl ester	21.17
2-((2-Methoxyethoxy)carbonyl)benzoic acid	22.36
4-Isopropyl-5-methylhexa-2,4-dien-1-ol	22.99
Sulfurous acid, hexyl octyl ester	24.18
Fumaric acid, 2-isopropylphenyl pentadecyl ester	24.56
1,3,5-Trimethyl-3,7-diazabicyclo[3.3.1]nonan-9-ol	25.15
1,3,5-Triazin-2-amine, 4,6-dichloro-N,N-diethyl	26.43
Methyl stearate	26.67
Heptadecanoic acid, methyl ester	27.39
1,4-Dithiin, 5-(1,1-dimethylethyl)-2,3-dihydro-, 1,1-dioxide	27.67
Dodecane, 2-methyl-6-propyl	27.91

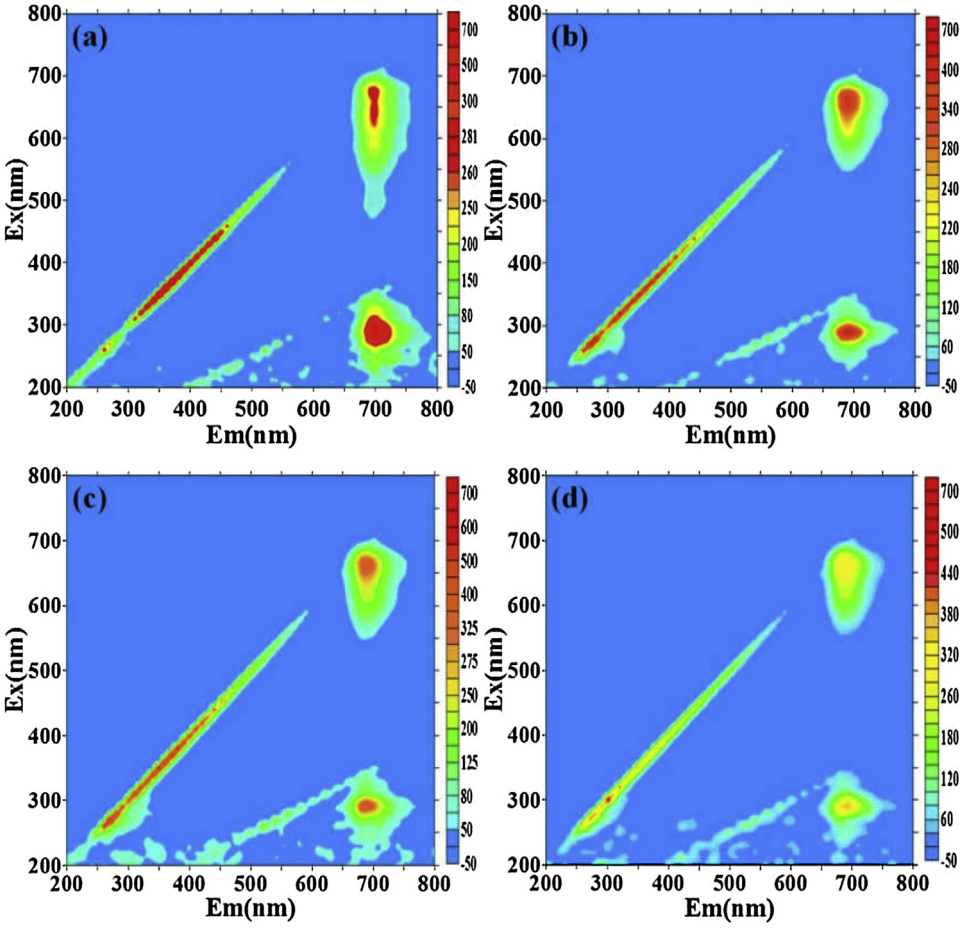

Fig. 6. (a) EEM fluorescence spectra of MB. EEM fluorescence spectra of MB over $Co_{2.67}S_4$ (b) after dark reaction one hour, (c) under NIR irradiation 60 min, (d) after the end of the near-infrared irradiation time 120 min.

transition of electrons from the valence band to the conduction band, leaving an equal number of holes in the valence band. Then, the excited electrons and holes transferred to the surface. The external photogenerated electrons or holes could generated a series of reactive medial species for destruction of dye molecules [52]. Ordinarily, the photogenerated electrons were captured by dissolved oxygen, and afterwards superoxide radical anions ($^{\bullet}O_2^-$) would be acquired first, followed by constitution of other active species containing hydroxyl radical ($^{\bullet}OH$) and others [53,54]. All these reactive oxygen species possessed sufficient energy for oxidation of pollutants. In this case, owing to a bandgap excitation edge at 400 nm of $Co_{2.67}S_4$ (Fig. 5a), above-mentioned essential mechanism can well make an interpretation on the photocatalytic activity of $Co_{2.67}S_4$ under UV irradiation.

In order to investigate possible photocatalytic mechanism under NIR irradiation, a series of scavengers were introduced to eliminate the relevant active species. Firstly, after 120 min illumination in N_2-saturated condition, the photocatalytic conversion ratio of MB had been reduced to nearly 49% (Fig. 7). Compared with the curve without scavengers addition, the decrease of photocatalytic efficiency was that the $^{\bullet}O_2^-$ might not be generated under N_2-saturated condition, when the oxygen was dispelled from the reaction system. Moreover, O_2 could be as an electron-capturer to produce $^{\bullet}O_2^-$, which was a very important active species in the photocatalytic process. Therefore, O_2 was extremely important in the photocatalytic reaction, and oxygen content in the air was enough for the photodegradation [55]. Alternatively, 1.0 mM sodium oxalate as a hole-capturer was added in the system. The addition of the hole scavenger had weakened the photocatalytic activity of $Co_{2.67}S_4$ for the degradation of MB to almost 46%. The phenomenon could be explained by the strong oxidation ability of holes, which can oxidize H_2O to $^{\bullet}OH$ [55]. Moreover, isopropanol was used for quenching $^{\bullet}OH$ [56]. Notably when the isopropanol (1.0 mM) was added, the photocatalytic conversion ratio had been decreased. It illustrated that $^{\bullet}OH$ was generated and played an important role in the reaction system.

According to the experimental information above, a plausible mechanism was put forward to interpret the reasons why $Co_{2.67}S_4$

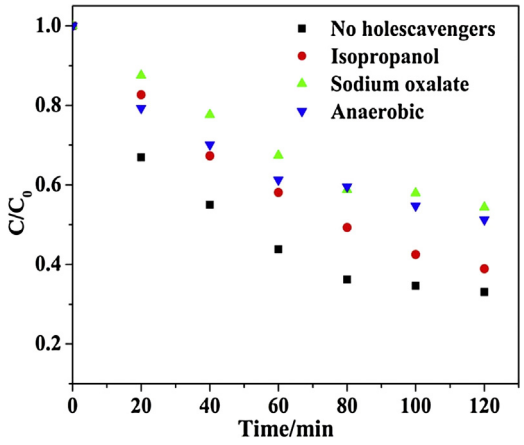

Fig. 7. Effects of different reactive species scavengers on the photodegradation of MB by $Co_{2.67}S_4$ under near-infrared light irradiation.

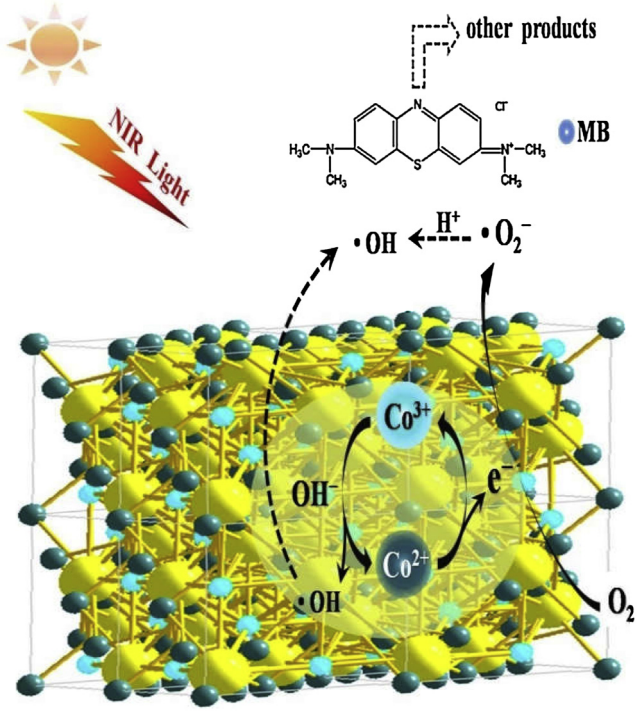

Fig. 8. Illustrative diagram of the $Co_{2.67}S_4$ system under NIR light irradiation.

could give a NIR driven photocatalytic activity. The reaction equation had been shown as follows:

$$Co^{2+} + h\nu(NIR) \rightarrow Co^{3+*} + e^- \quad (1)$$

$$O_2 + e^- \rightarrow \cdot O_2^- \quad (2)$$

$$Co^{2+} + O_2 \rightarrow \cdot O_2^- + Co^{3+*} \quad (3)$$

$$\cdot O_2^- + H^+ \rightarrow \cdot OH \quad (4)$$

$$Co^{3+*} + OH^- \rightarrow Co^{2+} + \cdot OH \quad (5)$$

$$\cdot O_2^-, \cdot OH + MB \rightarrow \text{other products} \quad (6)$$

Moreover, the photocatalytic process of $Co_{2.67}S_4$ can also be schematically illustrated in Fig. 8. When $Co_{2.67}S_4$ nanoparticles was exposed to the NIR irradiation, Co^{2+} sites as chromophore or photosensitive sites were excited with photogenerated electrons and Co^{3+*} (Eq. (1)). Whereafter, photogenerated electrons would be captured by the absorbed O_2 to form $^{\bullet}O_2^-$, and Co^{2+} sites could also react with O_2 to form Co^{3+*} respectively, followed by the generation of $^{\bullet}OH$ (Eqs. (2)–(4)) [57]. Furthermore, the Co^{3+*} sites could react with OH^- and return to Co^{2+}, achieving a full photocatalytic circle (Eq. (5)). This phenomenon is an analogous instance to that of reported Cs_xWO_3, where valence alternation of tungsten ions was deemed to induce extinction of NIR light as well as played a vital role on NIR-driven photocatalytic activity [53]. Ultimately, the reactive species, including $^{\bullet}OH$ and $^{\bullet}O_2^-$ all possess ample energy for oxidation of dyes (Eq. (6)).

Finally, Co^{2+} ions may also be excited by visible light in an analogous way to that of Eq. (1), and resultantly account for the visible light driven photocatalytic activity of $Co_{2.67}S_4$.

4. Conclusions

In summary, $Co_{2.67}S_4$ nanoparticles, a novel full-spectrum-response photocatalysts was synthesized through a facile and efficient solvothermal route. It possessed great optical absorption in a broad range of 240–2200 nm, covering the UV, visible and NIR light region. The $Co_{2.67}S_4$ with mixed valence exhibited great photocatalytic ability for the degradation of MB under UV light (64% within 60 min), visible light (84% within 60 min) and near-infrared light (68% within 120 min). The Co^{2+}/Co^{3+} redox couple was the predominant mechanism in the photocatalytic process. The reactive species ($^{\bullet}O_2^-$, $^{\bullet}OH$) formed in the photocatalytic process led to the MB degradation. This discovery is of great significance for full utilization of solar energy, and opens a new door to harnessing full solar light for waste-water cleaning.

Acknowledgments

The authors were thankful for funds from the Foundation for Innovative Research Groups of the National Natural Science Foundation of China (No. 51521006), National Natural Science Foundation of China (No. 71431006, 21276069, 71221061)

References

[1] X. Chen, C. Li, M. Gratzel, R. Kostecki, S.S. Mao, Chem. Soc. Rev. 41 (2012) 7909–7937.
[2] Q. Zhang, C.S. Dandeneau, X. Zhou, G. Cao, Adv. Mater. 21 (2009) 4087–4108.
[3] S.K. Cushing, J. Li, F. Meng, T.R. Senty, S. Suri, M. Zhi, M. Li, A.D. Bristow, N. Wu, J. Am. Chem. Soc. 134 (2012) 15033–15041.
[4] H. Wang, X. Yuan, Y. Wu, H. Huang, X. Peng, G. Zeng, H. Zhong, J. Liang, M. Ren, Adv. Colloid Interface Sci. 195-196 (2013) 19–40.
[5] J. Di, J. Xia, M. Ji, B. Wang, S. Yin, H. Xu, Z. Chen, H. Li, Langmuir 32 (2016) 2075–2084.
[6] L. Zhang, W. Wang, S. Sun, D. Jiang, Appl. Catal. B: Environ. 168–169 (2015) 9–13.
[7] H. Wang, X. Yuan, G. Zeng, Y. Wu, Y. Liu, Q. Jiang, S. Gu, Adv. Colloid Interface Sci. 221 (2015) 41–59.
[8] S. Huang, S. Guo, Q. Wang, N. Zhu, Z. Lou, L. Li, A. Shan, H. Yuan, ACS Appl. Mater. Interfaces 7 (2015) 20170–20178.
[9] X. Zhang, B. Peng, T. Peng, L. Yu, R. Li, J. Zhang, J. Power Sources 298 (2015) 30–37.
[10] X. Zhang, L. Yu, C. Zhuang, T. Peng, R. Li, X. Li, ACS Catal. 4 (2014) 162–170.
[11] S. Huang, Z. Lou, Z. Qi, N. Zhu, H. Yuan, Appl. Catal. B: Environ. 168–169 (2015) 313–321.
[12] W. Qin, D. Zhang, D. Zhao, L. Wang, K. Zheng, Chem. Commun. 46 (2010) 2304–2306.
[13] X. Guo, C. Chen, S. Yin, W. Song, F. Shi, W. Qin, J. Photochem. Photobiol. A: Chem. 297 (2015) 14–19.
[14] X. Guo, W. Song, C. Chen, W. Di, W. Qin, Phys. Chem. Chem. Phys. 15 (2013) 14681–14688.
[15] W. Gao, W. Liu, Y. Leng, X. Wang, X. Wang, B. Hu, D. Yu, Y. Sang, H. Liu, Appl. Catal. B: Environ. 176–177 (2015) 83–90.
[16] M.Z. Huang, B. Yuan, L. Dai, M.L. Fu, J. Colloid Interface Sci. 460 (2015) 264–272.
[17] S. Huang, Y. Feng, L. Han, W. Fan, X. Zhao, Z. Lou, Z. Qi, B. Yu, N. Zhu, RSC Adv. 4 (2014) 61679–61686.
[18] S. Huang, Z. Lou, N. Zhu, H. Yuan, Catal. Commun. 61 (2015) 6–10.
[19] C. Li, F. Wang, J. Zhu, J.C. Yu, Appl. Catal. B: Environ. 100 (2010) 433–439.
[20] J. Méndez-Ramos, P. Acosta-Mora, J.C. Ruiz-Morales, N.M. Khaidukov, J. Alloys Compd. 575 (2013) 263–267.
[21] F. Wang, Y. Han, C.S. Lim, Y. Lu, J. Wang, J. Xu, H. Chen, C. Zhang, M. Hong, X. Liu, Nature 463 (2010) 1061–1065.
[22] G.S. Yi, G.M. Chow, Adv. Funct. Mater. 16 (2006) 2324–2329.
[23] Y. Zhang, Z. Hong, Nanoscale 5 (2013) 8930–8933.
[24] J. Tian, Y. Sang, G. Yu, H. Jiang, X. Mu, H. Liu, Adv. Mater. 25 (2013) 5075–5080.
[25] Y. Sang, Z. Zhao, M. Zhao, P. Hao, Y. Leng, H. Liu, Adv. Mater. 27 (2015) 363–369.
[26] S.J. Bao, Y.B. Li, C.M. Li, Q.L. Bao, Q. Lu, J. Guo, Cryst. Growth Des. 8 (2008) 3745–3749.
[27] S. Kong, Z. Jin, H. Liu, Y. Wang, J. Phys. Chem. C 118 (2014) 25355–25364.
[28] S. Peng, L. Li, S.G. Mhaisalkar, M. Srinivasan, S. Ramakrishna, Q. Yan, ChemSusChem 7 (2014) 2212–2220.
[29] B.T. Yonemoto, G.S. Hutchings, F. Jiao, J. Am. Chem. Soc. 136 (2014) 8895–8898.
[30] N. Mahmood, C. Zhang, J. Jiang, F. Liu, Y. Hou, Chemistry 19 (2013) 5183–5190.
[31] H. Emadi, M. Salavati-Niasari, F. Davar, Polyhedron 31 (2012) 438–442.
[32] W.W. Zhao, C. Zhang, F.Y. Geng, S.F. Zhuo, B. Zhang, ACS Nano 8 (2014) 10909–10919.
[33] Q. Liu, J. Zhang, CrystEngComm 15 (2013) 5087.
[34] M. Xu, H. Niu, J. Huang, J. Song, C. Mao, S. Zhang, C. Zhu, C. Chen, Appl. Surf. Sci. 351 (2015) 374–381.
[35] Z. Yang, C.-Y. Chen, H.-T. Chang, Sol. Energy Mater. Sol. Cells 95 (2011) 2867–2873.
[36] S. Das, P. Sudhagar, S. Nagarajan, E. Ito, S.Y. Lee, Y.S. Kang, W. Choi, Carbon 50 (2012) 4815–4821.

[37] H. Wang, X. Yuan, H. Wang, X. Chen, Z. Wu, L. Jiang, W. Xiong, G. Zeng, Appl. Catal. B: Environ. 193 (2016) 36–46.
[38] Q. Jiang, X. Yuan, H. Wang, X. Chen, S. Gu, Y. Liu, Z. Wu, G. Zeng, RSC Adv. 5 (2015) 53019–53024.
[39] Y. Liu, X. Yuan, H. Wang, X. Chen, S. Gu, Q. Jiang, Z. Wu, L. Jiang, Y. Wu, G. Zeng, Catal. Commun. 70 (2015) 17–20.
[40] H. Wang, X. Yuan, Y. Wu, X. Chen, L. Leng, G. Zeng, RSC Adv. 5 (2015) 32531–32535.
[41] H. Wang, X. Yuan, Y. Wu, G. Zeng, H. Dong, X. Chen, L. Leng, Z. Wu, L. Peng, Appl. Catal. B: Environ. 186 (2016) 19–29.
[42] X. Yuan, H. Wang, Y. Wu, X. Chen, G. Zeng, L. Leng, C. Zhang, Catal. Commun. 61 (2015) 62–66.
[43] Z. Wu, H. Zhong, X. Yuan, H. Wang, L. Wang, X. Chen, G. Zeng, Y. Wu, Water Res. 67 (2014) 330–344.
[44] X.H. Chen, R. Fan, Chem. Mater. 13 (2001) 802–805.
[45] H. Zhang, L.V. Solomon, D.H. Ha, S. Honrao, R.G. Hennig, R.D. Robinson, Dalton Trans. 42 (2013) 12596–12599.
[46] V. Kozhukharov, M. Machkova, P. Ivanov, H.J.M. Bouwmeester, R. Van Doorn, J. Mater. Sci. Lett. 15 (1996) 1727–1729.
[47] B. Liu, D. Kong, J. Zhang, Y. Wang, T. Chen, C. Cheng, H.Y. Yang, J. Mater. Chem. A 4 (2016) 3287–3296.
[48] P. Sennu, M. Christy, V. Aravindan, Y.-G. Lee, K.S. Nahm, Y.-S. Lee, Chem. Mater. 27 (2015) 5726–5735.
[49] Y. Du, X. Zhu, X. Zhou, L. Hu, Z. Dai, J. Bao, J. Mater. Chem. A 3 (2015) 6787–6791.
[50] H. Hua, S. Liu, Z. Chen, R. Bao, Y. Shi, L. Hou, G. Pang, K.N. Hui, X. Zhang, C. Yuan, Sci. Rep. 6 (2016) 20973.
[51] H. Li, R. Liu, Y. Liu, H. Huang, H. Yu, H. Ming, S. Lian, S.-T. Lee, Z. Kang, J. Mater. Chem. 22 (2012) 17470.
[52] D.-X. Xu, Z.-W. Lian, M.-L. Fu, B. Yuan, J.-W. Shi, H.-J. Cui, Appl. Catal. B: Environ. 142–143 (2013) 377–386.
[53] G. Li, C. Guo, M. Yan, S. Liu, Appl. Catal. B: Environ. 183 (2016) 142–148.
[54] H. Tong, S.X. Ouyang, Y.P. Bi, N. Umezawa, M. Oshikiri, J.H. Ye, Adv. Mater. 24 (2012) 229–251.
[55] S. Meng, D. Li, M. Sun, W. Li, J. Wang, J. Chen, X. Fu, G. Xiao, Catal. Commun. 12 (2011) 972–975.
[56] Y.R. Jiang, H.P. Lin, W.H. Chung, Y.M. Dai, W.Y. Lin, C.C. Chen, J. Hazard. Mater. 283 (2015) 787–805.
[57] P. Wang, Y. Tang, Z. Dong, Z. Chen, T.-T. Lim, J. Mater. Chem. A 1 (2013) 4718.